# Weierstraß-Institut
## für Angewandte Analysis und Stochastik

im Forschungsverbund Berlin e.V.

Preprint ISSN 0946 – 8633


# Surface Waves in Two-Component Poroelastic Media on Impermeable Boundaries – Numerical Analysis in the Whole Frequency Domain


Bettina Albers



submitted: 15th August 2003



Weierstrass Institute
for Applied Analysis
and Stochastics
Mohrenstr. 39
10117 Berlin
Germany
E-Mail: albers@wias-berlin.de



No. 862
Berlin 2003


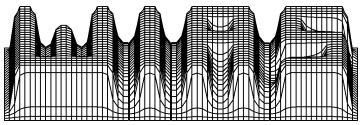


2000 *Mathematics Subject Classification.* 74J15, 76S05, 74S99.

*Key words and phrases.* Surface waves, flows in porous media, numerical analysis of dispersion relation.

Edited by
Weierstraß-Institut für Angewandte Analysis und Stochastik (WIAS)
Mohrenstraße 39
D — 10117 Berlin
Germany

Fax: + 49 30 2044975
E-Mail: preprint@wias-berlin.de
World Wide Web: http://www.wias-berlin.de/

**Abstract**

In this work the dispersion relation for surface waves on an impermeable boundary of a fully saturated poroelastic medium is investigated numerically in the whole range of frequencies. A linear model of a two-component poroelastic medium is used in the form proposed by K. Wilmański in [12]. Similarly to the classical Biot's model [3] it is a continuum mechanical model but it is much simpler.

In the whole range of frequencies there exist two modes of surface waves corresponding to the classical Rayleigh and Stoneley waves. The numerical results for velocities and attenuations of these waves are shown for different values of the bulk permeability coefficient, $\pi$, in different ranges of frequencies.

# 1 Introduction

The theoretical investigation of surface waves in porous materials is motivated by the construction of a method of nondestructive testing of such systems as

- soils and rocks,
- concrete and other porous construction materials,
- road surface and pavement,
- bones and soft tissues such as the surface of the heart,
- surface coating by nanomaterials.

In most cases of practical interest in soil mechanics the range of applicable frequencies lies between 1 Hz and 100 Hz. However, some medical applications, for instance, allow for higher frequencies up to app. 3 MHz while testing of nanomaterials requires frequencies of app. 100 MHz. The classical approach to the propagation of surface waves is based on one-component elastic models in the limit $\omega \to \infty$. Then, solely a so-called Rayleigh wave appears [11]. However, according to the above remark on soil mechanics, the other limit: $\omega \to 0$ for heterogeneous elastic solids has to be applied and, particularly, the inverse problem for low frequencies is investigated [9], [10].

One of the first attempts to investigate surface waves in two-component porous materials stems from Deresiewicz [5]. An extensive analysis for Biot's model in

the range of high frequencies was carried by Feng & Johnson [8]. They show some basic properties of surface waves in a high-frequency approximation by means of a numerical technique. They have investigated additional modes of surface waves in dependence on the permeability of the boundary and on the coefficient of added mass ("tortuosity") in different ranges of the stiffness of the skeleton.

In this work we rely on a simpler model than this of Biot. We neglect two effects:

- an added mass effect reflected in the Biot's model by off-diagonal contributions to the matrix of partial mass densities,
- a static coupling effect between partial stresses.

The first contribution is neglected because it yields a non-objectivity of Biot's equations (see e.g. [13]). This does not mean that the tortuosity may not have an influence on the propagation of surface waves but solely that it is not modelled in the right way by Biot. Incidentally, the conclusion on the existence of three surface modes for impermeable boundaries ($T \to \infty$ in [8]) contradicts the basic principle of the linear system describing three body waves ($P1, P2, S$). These may combine only into two surface modes. The third surface mode in the work [8] is apparently related to $\alpha \neq 0$ supposedly describing the tortuosity.

The second contribution is neglected because it yields small quantitative changes (app. 5%) [16] and does not influence spectral qualitative properties of surface waves. Consequently, the model becomes simpler and its high-frequency properties for surface waves seem to be physically correct (see e.g. [7] where they were investigated by means of an asymptotic analysis of the dispersion relation in function of the wavelength $1/k$, $k$ – wave number).

The purpose of this work is to investigate the dispersion relation for surface waves on an impermeable boundary of a fully saturated poroelastic medium in the *whole range* of frequencies.

In the next section we present the linear form of the model for a two-component poroelastic saturated medium. We show the governing equations and, briefly, the construction of the solution for a semiinfinite medium with an impermeable boundary. Section 2.2.4 is devoted to the presentation of the boundary conditions on such an interface between a porous medium and a vacuum. Afterwards we show the general dispersion relation and summarize results of an earlier work for the high and low frequency approximations. The main part of the paper concerns numerical aspects: first we indicate the applied numerical procedure and then we illustrate the numerical results for the normalized velocities and attenuations of the Rayleigh and Stoneley waves. It is known that surface modes of propagation in linear models result from the combination of bulk modes. Physically, this means that at any point of the boundary classical longitudinal and shear waves combine into the Rayleigh

wave which must be slower than both bulk waves. The presence of the second longitudinal bulk wave $P2$ yields the existence of the second surface mode – the Stoneley wave which should be slower than the P2-wave – the slowest of bulk waves. Both quantities, velocities and attenuations, are shown for different values of the bulk permeability coefficient, $\pi$, in different ranges of frequencies. A decay of the Rayleigh wave velocity, mentioned in the book [4] (p. 265) has been confirmed in the range of small frequencies in spite of the lack of static coupling between components. As it is very small it may not be observable experimentally. It is claimed in the above book that the decay results from an influence of the $P2$-wave. Moreover we compare the behaviour of the two types of surface waves with the behaviour of two bulk waves: $P1$, and $P2$.

# 2 Model

In this section we present a linear model of a two-component poroelastic saturated medium. (see e.g. [12]).

## 2.1 Governing equations

Within this model the process is described by the *macroscopic* fields $\rho^F(\mathbf{x},t)$ – partial mass density of the fluid, $\mathbf{v}^F(\mathbf{x},t)$ – velocity of the fluid, $\mathbf{v}^S(\mathbf{x},t)$ – velocity of the skeleton, $\mathbf{e}^S(\mathbf{x},t)$ – symmetric tensor of small deformations of the skeleton and the porosity $n$. These fields satisfy the following set of linear equations

$$
\begin{aligned}
&\frac{\partial \rho^F}{\partial t} + \rho_0^F \operatorname{div} \mathbf{v}^F = 0, \quad \left| \frac{\rho^F - \rho_0^F}{\rho_0^F} \right| \ll 1, \\
&\rho_0^F \frac{\partial \mathbf{v}^F}{\partial t} + \kappa \operatorname{grad} \rho^F + \beta \operatorname{grad}\,(n - n_E) + \hat{\mathbf{p}} = 0, \quad \hat{\mathbf{p}} := \pi \left( \mathbf{v}^F - \mathbf{v}^S \right), \\
&\rho_0^S \frac{\partial \mathbf{v}^S}{\partial t} - \operatorname{div} \left( \lambda^S \left( \operatorname{tr} \mathbf{e}^S \right) \mathbf{1} + 2\mu \mathbf{e}^S + \beta\,(n - n_E)\,\mathbf{1} \right) - \hat{\mathbf{p}} = 0, \\
&\frac{\partial \mathbf{e}^S}{\partial t} = \operatorname{sym} \operatorname{grad} \mathbf{v}^S, \quad \left\| \mathbf{e}^S \right\| \ll 1, \quad n_E := n_0 \left( 1 + \delta \operatorname{tr} \mathbf{e}^S \right), \\
&\frac{\partial\,(n - n_E)}{\partial t} + \Phi \operatorname{div} \left( \mathbf{v}^F - \mathbf{v}^S \right) + \frac{n - n_E}{\tau} = 0, \quad \left| \frac{n - n_0}{n_0} \right| \ll 1.
\end{aligned}
\tag{1}
$$

Here $\rho_0^F, \rho_0^S, n_0$ denote constant reference values of partial mass densities, and porosity, respectively, and $\kappa, \lambda^S, \mu^S, \beta, \pi, \tau, \delta, \Phi$ are constant material parameters. The first one describes the macroscopic compressibility of the fluid component, the next two are macroscopic elastic constants of the skeleton, $\beta$ is the coupling constant, $\pi$ is the coefficient of bulk permeability, $\tau$ is the relaxation time and $\delta$, $\Phi$ describe equilibrium and nonequilibrium changes of porosity, respectively. For the purpose of this work we assume $\beta = 0$. Then the problem of evolution of porosity described

by equation $(1)_5$ can be solved separately from the rest of the problem and does not influence the propagation of acoustic waves in the medium.

## 2.2 Construction of solution for a semiinfinite medium with impermeable boundary

We follow here the same procedure of construction of solutions as in the works [15], [7] and [17]. In contrast to some earlier works on this model, here, we consider solely monochromatic waves with a given *real frequency* $\omega$. This may be considered either as a Fourier component of the expansion of the solution in time space or as a far field boundary value problem with a harmonic surface source of waves.

### 2.2.1 Compatibility with field equations

We introduce the displacement vector $\mathbf{u}^S$ for the skeleton, and formally the displacement vector $\mathbf{u}^F$ for the fluid. The latter is introduced solely for the technical symmetry of considerations and does not have any physical bearing. Then

$$\begin{aligned} \mathbf{u}^S &= \operatorname{grad}\varphi^S + \operatorname{rot}\psi^S, \quad \mathbf{v}^S = \frac{\partial \mathbf{u}^S}{\partial t}, \quad \mathbf{e}^S = \operatorname{sym}\operatorname{grad}\mathbf{u}^S, \\ \mathbf{u}^F &= \operatorname{grad}\varphi^F + \operatorname{rot}\psi^F, \quad \mathbf{v}^F = \frac{\partial \mathbf{u}^F}{\partial t}. \end{aligned} \tag{2}$$

For the two-dimensional case[1] we make the following ansatz for monochromatic wave solutions in the $x$-direction

$$\begin{aligned} \varphi^S &= A^S(z)\exp\left[i\left(kx-\omega t\right)\right], \quad \varphi^F = A^F(z)\exp\left[i\left(kx-\omega t\right)\right], \\ \psi_z^S &= B^S(z)\exp\left[i\left(kx-\omega t\right)\right], \quad \psi_z^F = B^F(z)\exp\left[i\left(kx-\omega t\right)\right], \\ \psi_x^S &= \psi_y^S = \psi_x^F = \psi_y^F = 0, \end{aligned} \tag{3}$$

and

$$\rho^F - \rho_0^F = A_\rho^F(z)\exp\left[i\left(kx-\omega t\right)\right]. \tag{4}$$

Substitution in field equations (1) leads after straightforward calculations to the following compatibility conditions

$$B^F = \frac{i\pi}{\rho_0^F\omega + i\pi}B^S, \quad A_\rho^F = -\rho_0^F\left(\frac{d^2}{dz^2} - k^2\right)A^F, \tag{5}$$

as well as

[1] Under this assumption we are not able to describe the geometrical dispersion of waves which is the main practical motivation for surface waves in contrast to bulk waves. The attenuation of waves calculated in this work follows solely from the dissipation caused by diffusion.

$$\left[\kappa\left(\frac{d^2}{dz^2}-k^2\right)+\omega^2\right]A^F+\frac{i\pi}{\rho_0^F}\omega\left(A^F-A^S\right)=0, \tag{6}$$

$$\left[\frac{\lambda^S+2\mu^S}{\rho_0^S}\left(\frac{d^2}{dz^2}-k^2\right)+\omega^2\right]A^S-\frac{i\pi}{\rho_0^S}\omega\left(A^F-A^S\right)=0, \tag{7}$$

$$\left[\frac{\mu^S}{\rho_0^S}\left(\frac{d^2}{dz^2}-k^2\right)+\omega^2+\frac{i\pi\rho_0^F}{\rho_0^S\left(\rho_0^F\omega+i\pi\right)}\omega^2\right]B^S=0. \tag{8}$$

### 2.2.2 Dimensionless notation

It is convenient to introduce a dimensionless notation. Therefore we define the following dimensionless quantities

$$\begin{aligned} &c_s:=\frac{c_S}{c_{P1}}<1, \quad c_f:=\frac{c_{P2}}{c_{P1}}, \quad \pi':=\frac{\pi\tau}{\rho_0^S}>0, \\ &r:=\frac{\rho_0^F}{\rho_0^S}<1, \qquad z':=\frac{z}{c_{P1}\tau}, \quad k':=kc_{P1}\tau, \quad \omega':=\omega\tau, \end{aligned} \tag{9}$$

where $c_{P1}, c_S, c_{P2}$ are defined by the relations

$$c_{P1}:=\sqrt{\frac{\lambda^S+2\mu^S}{\rho_0^S}}, \quad c_{P2}:=\sqrt{\kappa}, \quad c_S:=\sqrt{\frac{\mu^S}{\rho_0^S}}. \tag{10}$$

These are the front velocities of the three bulk waves in a two-component porous medium: Two longitudinal waves, $P1$ (fast wave) and $P2$ (slow wave, also called Biot's wave), and one shear wave, $S$. In the case of Biot's model there would be an additive contribution in the numerator of $c_{P1}$ of the coupling parameter $Q$ which is of the order of a few percent of $\lambda^S$.

### 2.2.3 Ansatz

Further we omit the prime for typographical reasons. Substitution of (9) in equations (6), (7), (8) yields

$$\begin{aligned} \left[c_f^2\left(\frac{d^2}{dz^2}-k^2\right)+\omega^2\right]A^F+i\frac{\pi}{r}\omega\left(A^F-A^S\right) &= 0, \\ \left[\left(\frac{d^2}{dz^2}-k^2\right)+\omega^2\right]A^S-i\pi\omega\left(A^F-A^S\right) &= 0, \\ \left[c_s^2\left(\frac{d^2}{dz^2}-k^2\right)+\omega^2+\frac{i\pi\omega^2}{\omega+i\frac{\pi}{r}}\right]B^S &= 0. \end{aligned} \tag{11}$$

The matrix of coefficients for homogeneous materials is independent of $z$. Hence the differential eigenvalue problem can be easily solved. Consequently we seek solutions in the form

$$A^F = A_f^1 e^{\gamma_1 z} + A_f^2 e^{\gamma_2 z}, \quad A^S = A_s^1 e^{\gamma_1 z} + A_s^2 e^{\gamma_2 z}, \quad B^S = B_s e^{\zeta z}. \tag{12}$$

Substitution in (11) yields relations for the exponents in the form

$$\left(\frac{\zeta}{k}\right)^2 = 1 - \frac{1}{c_s^2}\left(1 + \frac{i\pi}{\omega + i\frac{\pi}{r}}\right)\left(\frac{\omega}{k}\right)^2, \tag{13}$$

and

$$\begin{aligned} &c_f^2\left[\left(\frac{\gamma}{k}\right)^2 - 1\right]^2 + \left[1 + \left(1 + \frac{1}{r}\right)\frac{i\pi}{\omega}\right]\left(\frac{\omega}{k}\right)^4 \\ &+ \left[1 + c_f^2 + \left(c_f^2 + \frac{1}{r}\right)\frac{i\pi}{\omega}\right]\left[\left(\frac{\gamma}{k}\right)^2 - 1\right]\left(\frac{\omega}{k}\right)^2 = 0. \end{aligned} \tag{14}$$

Simultaneously we obtain for the eigenvectors the following relations

$$\mathbf{R}^1 = \left(B_s, A_s^1, A_f^1\right)^T, \quad \mathbf{R}^2 = \left(B_s, A_s^2, A_f^2\right)^T, \tag{15}$$

where

$$A_f^1 = \delta_f A_s^1, \quad A_s^2 = \delta_s A_f^2, \tag{16}$$

$$\delta_f := \frac{1}{r}\frac{\frac{i\pi}{\omega}\frac{\omega^2}{k^2}}{c_f^2\left[\left(\frac{\gamma_1}{k}\right)^2 - 1\right] + \left(\frac{\omega}{k}\right)^2 + \frac{i\pi}{\omega r}\frac{\omega^2}{k^2}}, \tag{17}$$

$$\delta_s := \frac{\frac{i\pi}{\omega}\frac{\omega^2}{k^2}}{\left(\frac{\gamma_2}{k}\right)^2 - 1 + \left(\frac{\omega}{k}\right)^2 + \frac{i\pi}{\omega}\frac{\omega^2}{k^2}}. \tag{18}$$

The above solution for the exponents still leaves three unknown constants $B_s, A_f^2, A_s^1$ which must be specified from boundary conditions.

### 2.2.4 Boundary conditions

In order to determine surface waves in a saturated poroelastic medium we need conditions for $z = 0$. In the general case of a boundary between a saturated porous material and a fluid the boundary conditions were formulated by Deresiewicz &

Skalak [6]. We quote them here in a slightly modified form. If we denote quantities outside of the porous medium by a "+" sign the boundary conditions have the form

$$
\begin{aligned}
&\bullet \quad \left(T_{13} - T_{13}^{+}\right)\Big|_{z=0} \equiv T_{13}^{S}\Big|_{z=0} = \mu^{S}\left(\frac{\partial u_1^S}{\partial z} + \frac{\partial u_3^S}{\partial x}\right)\Bigg|_{z=0} = 0, \\
&\bullet \quad \left(T_{33} - T_{33}^{+}\right)\Big|_{z=0} \equiv \left(T_{33}^{S} + p^{F+} - p^{F}\right)\Big|_{z=0} = \\
&\qquad = c_{P1}^2 \rho_0^S \left(\frac{\partial u_1^S}{\partial x} + \frac{\partial u_3^S}{\partial z}\right) - 2c_S^2 \rho_0^S \frac{\partial u_1^S}{\partial x} + \\
&\qquad + \kappa^{+}\left(\rho^{F+} - \rho_0^{F+}\right) - \kappa\left(\rho^{F} - \rho_0^{F}\right)\Big|_{z=0} = 0, \qquad (19) \\
&\bullet \quad \rho_0^F \frac{\partial}{\partial t}\left(u_3^F - u_3^S\right)\Bigg|_{z=0} = \rho_0^{F+} \frac{\partial}{\partial t}\left(u_3^{F+} - u_3^S\right)\Bigg|_{z=0}, \\
&\bullet \quad \rho_0^F \frac{\partial}{\partial t}\left(u_3^F - u_3^S\right) + \alpha\left(p^F - n_0 p^{F+}\right)\Big|_{z=0} = 0,
\end{aligned}
$$

where $u_1^S, u_3^S$ are $x$-, and $z$-components of the displacement $\mathbf{u}^S$, respectively, and $u_3^F, u_3^{F+}$ are $z$-components of the displacements $\mathbf{u}^F$ and $\mathbf{u}^{F+}$, respectively.

The first two conditions describe the continuity of the full traction, $\mathbf{t} := \left(\mathbf{T}^S + \mathbf{T}^F\right)\mathbf{n}$, $\mathbf{n} = (0,0,1)^T$, on the boundary; the third condition is the continuity of the fluid mass flux, and the last condition specifies the mass transport through the surface. The in- and outflow through the boundary is proportional to the difference of the pore pressures on both sides of the boundary. In this condition $\alpha$ denotes a surface permeability coefficient and $p^{F+}$ is the external pressure. This condition relies on the assumption that the pore pressure $p$ and the partial pressure $p^F$ satisfy the relation $p^F \approx n_0 p$ at least in a small vicinity of the surface.

For the impermeable boundary, for which $\alpha = 0$, the above boundary conditions simplify to the following ones

$$
\begin{aligned}
&\bullet \quad T_{13}\big|_{z=0} \equiv T_{13}^{S}\Big|_{z=0} = \mu^{S}\left(\frac{\partial u_1^S}{\partial z} + \frac{\partial u_3^S}{\partial x}\right)\Bigg|_{z=0} = 0, \qquad (20) \\
&\bullet \quad T_{33}\big|_{z=0} \equiv \left(T_{33}^{S} - p^{F}\right)\Big|_{z=0} = \\
&\qquad = c_{P1}^2 \rho_0^S \left(\frac{\partial u_1^S}{\partial x} + \frac{\partial u_3^S}{\partial z}\right) - 2c_S^2 \rho_0^S \frac{\partial u_1^S}{\partial x} + \qquad (21) \\
&\qquad -\kappa\left(\rho^{F} - \rho_0^{F}\right)\Big|_{z=0} = 0, \\
&\bullet \quad \frac{\partial}{\partial t}\left(u_3^F - u_3^S\right)\Bigg|_{z=0} = 0, \qquad (22)
\end{aligned}
$$

due to the fact that the quanities outside of the porous medium are equal to zero. Then the third and the fourth boundary conditions are identical. Let us mention here that the problem with permeable boundaries will be the topic of a forthcoming paper.

### 2.2.5 Dispersion relation

Substitution of the above results in the boundary conditions (20)-(22) yields the following equations for the three unknown constants $B_s, A_f^2$ and $A_s^1$

$$\mathbf{A}\mathbf{X} = \mathbf{0}, \tag{23}$$

where

$$\mathbf{A} := \begin{pmatrix} \left(\frac{\zeta}{k}\right)^2 + 1 & 2i\frac{\gamma_2}{k}\delta_s & 2i\frac{\gamma_1}{k} \\ -2ic_s^2\frac{\zeta}{k} & \left[\left(\frac{\gamma_2}{k}\right)^2 - 1 + 2c_s^2\right]\delta_s + \\ & \quad + rc_f^2\left[\left(\frac{\gamma_2}{k}\right)^2 - 1\right] & \left(\frac{\gamma_1}{k}\right)^2 - 1 + 2c_s^2 + \\ & & \quad + rc_f^2\left[\left(\frac{\gamma_1}{k}\right)^2 - 1\right]\delta_f \\ i\frac{r\omega}{r\omega + i\pi} & -(\delta_s - 1)\frac{\gamma_2}{k} & (\delta_f - 1)\frac{\gamma_1}{k} \end{pmatrix}, \tag{24}$$

$$\mathbf{X} := \begin{pmatrix} B_s, & A_f^2, & A_s^1 \end{pmatrix}^T.$$

This homogeneous set yields the *dispersion relation:* $\det \mathbf{A} = 0$ determining the $\omega - k$ relation. We investigate the numerical solution of this equation and compare the results for high and low frequencies with approximations shown in [17]. These are briefly summarized in the next subsection.

### 2.2.6 High and low frequency approximations

**High frequencies** In the limit $\omega \to \infty$ we immediately obtain from relations (13) and (14)

$$\left(\frac{\zeta}{k}\right)^2 = 1 - \frac{1}{c_s^2}\left(\frac{\omega}{k}\right)^2,$$
$$\left(\frac{\gamma_1}{k}\right)^2 = 1 - \left(\frac{\omega}{k}\right)^2, \quad \left(\frac{\gamma_2}{k}\right)^2 = 1 - \frac{1}{c_f^2}\left(\frac{\omega}{k}\right)^2, \tag{25}$$

and

$$\delta_f = \delta_s = 0 \quad \Rightarrow \quad \mathbf{R}^1 = \left(B_s, A_s^1, 0\right)^T, \quad \mathbf{R}^2 = \left(B_s, 0, A_f^2\right)^T. \tag{26}$$

The dispersion relation follows in the form

$$\mathcal{P}_R\sqrt{1 - c_f^2\left(\frac{\omega}{k}\right)^2} + \frac{r}{c_s^4}\left(\frac{\omega}{k}\right)^4\sqrt{1 - \left(\frac{\omega}{k}\right)^2} = 0, \tag{27}$$

where

$$\mathcal{P}_R := \left(2 - \frac{1}{c_s^2}\left(\frac{\omega}{k}\right)^2\right)^2 - 4\sqrt{1 - \left(\frac{\omega}{k}\right)^2}\sqrt{1 - \frac{1}{c_s^2}\left(\frac{\omega}{k}\right)^2}. \tag{28}$$

Hence for $r = 0$ the relation (27) reduces to $\mathcal{P}_R = 0$ which is the Rayleigh dispersion relation for single component continua.

**Low frequencies** For the limit $\omega \to 0$ one arrives at the following results for the first order approximation of exponents (notice a singularity of the last contribution to $\frac{\gamma_2}{k}$!)

$$\left(\frac{\zeta}{k}\right)^2 = 1 - \frac{r+1}{c_s^2}\left(\frac{\omega}{k}\right)^2,$$

$$\left(\frac{\gamma_1}{k}\right)^2 = 1 - \frac{r+1}{rc_f^2+1}\left(\frac{\omega}{k}\right)^2, \tag{29}$$

$$\left(\frac{\gamma_2}{k}\right)^2 = 1 - \frac{rc_f^4+1}{c_f^2\left(rc_f^2+1\right)}\left(\frac{\omega}{k}\right)^2 - \frac{i\pi}{\omega}\frac{rc_f^2+1}{rc_f^2}\left(\frac{\omega}{k}\right)^2,$$

and for the coefficients of amplitudes

$$\delta_f = 1 - \frac{\omega r}{i\pi}\frac{1-c_f^2}{1+rc_f^2}, \quad \delta_s = -rc_f^2\left(1 - \frac{\omega r}{i\pi}\frac{1-c_f^2}{1+rc_f^2}\right). \tag{30}$$

If we account for the relations (29) and (30) in the condition $\det \mathbf{A} = 0$ then we obtain a relation specifying $\frac{\omega}{k}$. From this we get as a solution a Rayleigh wave whose speed is given by a relation analogous to (28) in which the speeds of bulk waves (10) are replaced by their low frequency counterparts $c_{oP1}$ and $c_{oS}$:

$$\left(2 - \frac{c_{P1}^2}{c_{oS}^2}\left(\frac{\omega}{k}\right)^2\right)^2 - 4\sqrt{1 - \frac{c_{P1}^2}{c_{oS}^2}\left(\frac{\omega}{k}\right)^2}\sqrt{1 - \frac{c_{P1}^2}{c_{oP1}^2}\left(\frac{\omega}{k}\right)^2} = 0, \tag{31}$$

$$c_{oP1} := \sqrt{\frac{\lambda^S + 2\mu^S + \rho_0^F}{\rho_0^S + \rho_0^F}}, \qquad c_{oS} := \sqrt{\frac{\mu^S}{\rho_0^S + \rho_0^F}}.$$

In contrast to the high frequency approximation this wave is neither dispersive nor dissipative (no attenuation). The Stoneley wave does not exist in this approximation.

# 3 Numerical prodedure

The problem $\det \mathbf{A} = 0$ has been solved for the complex wave number, $k$, using the two computing packages MATLAB 5.3 and MAPLE V Release 5.1. The attempt to execute the calculation with the third package, MATHEMATICA 5, failed. In both successful packages, in principle, it is possible to use the existing equation solvers although they need for the calculations with complex variables very much of the main memory. It has been observed that the package MAPLE calculates solely *one of the solutions* for $k$ for any choice of sign combinations of exponents $\gamma_1, \gamma_2$ and $\zeta$, changing between branches of solution by the variation of exponents without any apparent reason. Sometimes it was the Rayleigh solution calculated

and sometimes the Stoneley solution. On the other hand, MATLAB revealed *all solutions* independently of a chosen combination of signs of exponents and this required testing any solution in order to find a corresponding combination of signs. Of course, the ascertained values agreed in both packages. The duration of the calculation for one value of $\omega$ was about 90s on a 1000 MHz machine.

From the complex results for $k$ we are able to determine the normalized velocities of the Rayleigh and Stoneley modes $c'_{Ra} = \dfrac{\omega}{\operatorname{Re} k_1}$, $c'_{St} = \dfrac{\omega}{\operatorname{Re} k_2}$, respectively, and the corresponding normalized attenuations $\operatorname{Im} k_1$ for the Rayleigh wave and $\operatorname{Im} k_2$ for the Stoneley wave.

Numerical solutions of the dispersion relation for controlled real $k$ and complex $\omega$ have not been constructed because, as well known, the solution for $P2$-waves and, consequently, for Stoneley waves becomes singular in the range of long waves (small $k$) (e.g. [1], [14]). Hence, such results seem to be solely of an academic interest.

# 4 Parameters

The results have been performed for the following numerical data

$$\beta = 0, \qquad c_{P1} = 2500\ \frac{\mathrm{m}}{\mathrm{s}}, \qquad c_{P2} = 1000\ \frac{\mathrm{m}}{\mathrm{s}}, \qquad c_S = 1500\ \frac{\mathrm{m}}{\mathrm{s}},$$

$$\rho_0^S = 2500\ \frac{\mathrm{kg}}{\mathrm{m}^3}, \qquad \rho_0^F = 250\ \frac{\mathrm{kg}}{\mathrm{m}^3}, \qquad c_s = \frac{c_S}{c_{P1}} = 0.6, \qquad c_f = \frac{c_{P2}}{c_{P1}} = 0.4,$$

$$r = \frac{\rho_0^F}{\rho_0^S} = 0.1, \qquad \pi = \begin{cases} 10^7\ \frac{\mathrm{kg}}{\mathrm{m}^3\mathrm{s}} \\ \text{or variable} \end{cases}, \qquad \tau = 10^{-6}\ \mathrm{s}, \qquad \pi' := \frac{\pi\tau}{\rho_0^S} = \begin{cases} 0.004 \\ \text{or variable} \end{cases}.$$

These data correspond approximately to, for instance, either marls or porous and saturated sandstones [4].

# 5 Numerical results

In the whole range of frequencies there exist two surface modes of propagation corresponding to the classical Rayleigh and Stoneley waves.

Results are shown for different values of the bulk permeability coefficient, $\pi$. This parameter describes the resistance of the porous medium against the flow of the fluid.

The classical form of the Darcy law refers to simple seepage experiments and describes the seepage velocity $v_S$ in terms of the pressure gradient

$$v_S = -\frac{K}{\rho g}\frac{dp}{dx},$$

where $\rho$ – mass density of the fluid, $g$ – earth acceleration, and $K$ – hydraulic conductivity.

This corresponds to the quasistatic form of the relation $(1)_2$

$$\frac{dp}{dx} + \pi\left(v^F - v^S\right) = 0.$$

Consequently the relation between permeability coefficients in these two approaches is as follows

$$\frac{K}{\rho g} \sim \frac{1}{\pi}.$$

For instance, for water saturated sands $K \sim 10^{-2} \div 10^{-3}\ \frac{\mathrm{m}}{\mathrm{s}}$, $\rho \sim 10^3\ \frac{\mathrm{kg}}{\mathrm{m}^3}$ and $g \sim 10\ \frac{\mathrm{m}}{\mathrm{s}^2} \Longrightarrow \pi \sim 10^6 \div 10^7\ \frac{\mathrm{kg}}{\mathrm{m}^3\mathrm{s}}$ (see e.g. [2]). In standard units of permeability this corresponds to app. $0.1 \div 1$ darcy.

## 5.1 Velocities of Rayleigh and Stoneley waves

Fig. 1 shows the velocity of the Rayleigh wave normalized by the $P1$-velocity in dependence on the frequency (see: (9)). The velocity is given for different values of the bulk permeability parameter $\pi$. The left and the right figure differ in the range of frequencies: While in the left one we see a range of frequencies from zero to the very large value of 100 MHz the right one shows a range from zero to 1 MHz. On the left figure we indicate additionally the high and low frequency limits common for all values of permeability, calculated according to section 2.2.6. We see that, indeed, the numerical results lie between these limits.

In the range of very small frequencies the velocity remains constant (independent of $\omega$) for all practical purposes. This range depends on the permeability and grows with growing $\pi$. There is an interesting small deviation from the constant value which we discuss later.

Simultaneously one can observe the selfsimilarity of curves for different values of $\pi$. This is due to the fact that $\pi$ and $\omega$ are normalized by the characteristic time $\tau$: $\omega' = \omega\tau$, $\pi' = \frac{\pi\tau}{\rho_0^S}$ and these are the only independent parameters which contain $\tau$. Certainly, as in the classical case of Rayleigh waves in a single component elastic medium, all values lie below the normalized velocity of the shear wave $c_s \equiv \frac{c_S}{c_{P1}} = 0.6$.

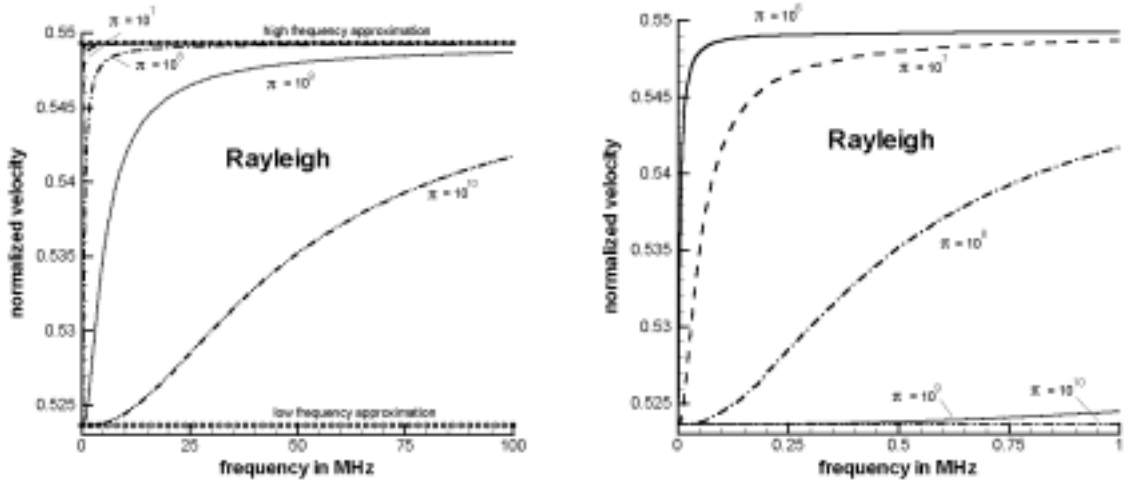


**Fig. 1:** Normalized velocities of the Rayleigh wave $c'_{Ra} \equiv \frac{c_{Ra}}{c_{P1}}$ for different values of the permeability coefficient $\pi$ in units $\left[\frac{\mathrm{kg}}{\mathrm{m^3 s}}\right]$ and in different ranges of frequencies. $c_s \equiv \frac{c_S}{c_{P1}} = 0.6$

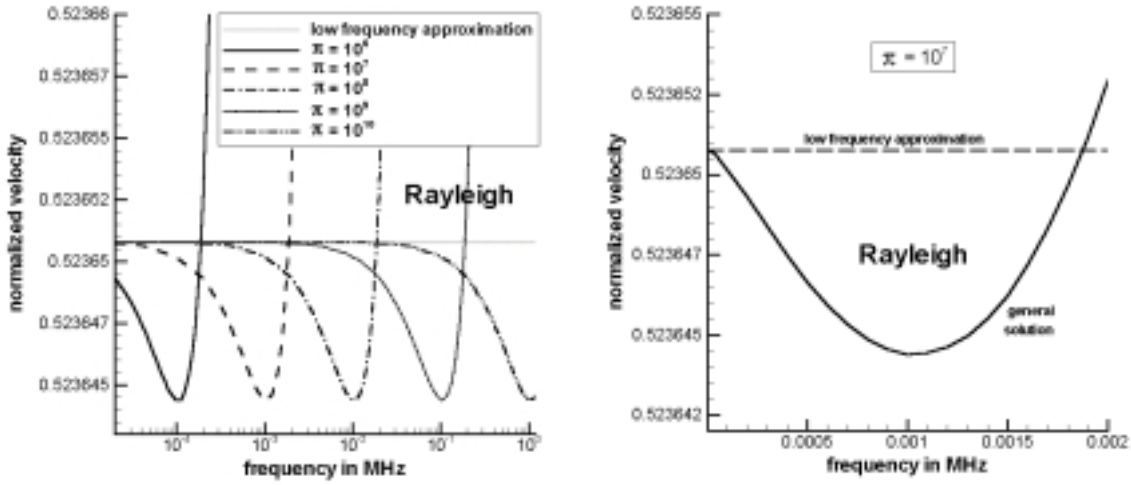


**Fig. 2:** Decay of the normalized Rayleigh velocity $\frac{c_{Ra}}{c_{P1}}$ in the range of relatively small frequencies. Left: for different values of the permeability coefficient $\pi$ in units $\left[\frac{\mathrm{kg}}{\mathrm{m^3 s}}\right]$, right: detail for $\pi = 10^7 \frac{\mathrm{kg}}{\mathrm{m^3 s}}$.

An interesting feature occurs for the velocity of the Rayleigh wave in the range of relatively small frequencies. This can be observed in a blow-up presented in Fig. 2. The Rayleigh velocity decays first a little and then it becomes growing to its limit value for $\omega \to \infty$. The maximum decay is very little indeed – app. 0.025% of the difference of limit values for $\omega = 0$ and $\omega \to \infty$. Interestingly, the minimum value remains constant for the different values of $\pi$. This means that the decay is not driven by the diffusion.

Bourbié, Coussy and Zinszner [4] prescribe this effect to an influence of the $P2$-wave, whose velocity is in this range very small. Consequently, it has a bigger influence than in the range of higher frequencies. It is interesting that this coupling is present in the simplified model where the coupling term in stresses is absent. Due to the latter property of the model the size of the effect is very small indeed, even though within the Biot's model it is not very large either (compare: Fig. 6.11 in [4], where the maximum corresponds to app. 0.3%).

In any case this region of the Rayleigh velocity has been investigated particularly carefully to eliminate the possibility of numerical artefacts.

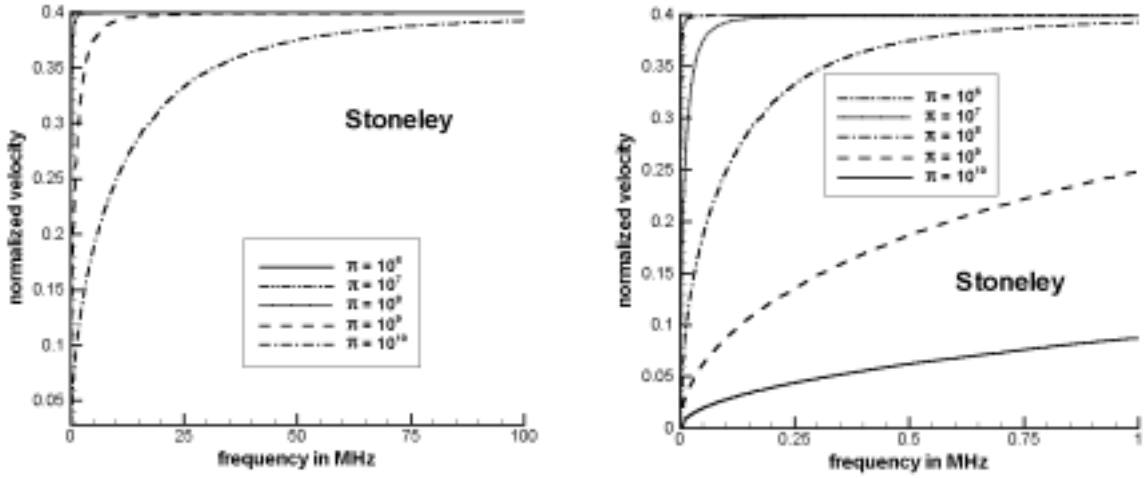


**Fig. 3:** Normalized velocities of the Stoneley wave $c'_{St} \equiv \frac{c_{St}}{c_{P1}}$ for different values of the permeability coefficient $\pi$ in units $\left[\frac{\mathrm{kg}}{\mathrm{m^3 s}}\right]$ in different ranges of frequencies.
$c_f \equiv \frac{c_{P2}}{c_{P1}} = 0.4$

In Fig. 3 we present the velocity of the Stoneley wave. It is normalized in the same way as the Rayleigh velocity. Also in these figures we see the curves for several values of $\pi$. The velocity increases from the zero value for $\omega = 0$. This property was indicated as a nonexistence of the Stoneley wave. The growth is faster than the growth of the Rayleigh velocity but the maximum value is smaller. It lies always below the normalized velocity of the fluid $c_f \equiv \frac{c_{P2}}{c_{P1}} = 0.4$. This happens for all values of $\pi$. The maximum value of the Stoneley velocity appearing for $\omega \to \infty$ is approximately 0.15% smaller than the velocity of the fluid. One should point out that the Stoneley velocity behaves regularly in the whole range of frequencies and it ceases to exist only for $\omega = 0$. In the vicinity of this point the Stoneley velocity possesses a similar feature to the P2-wave: it decays to zero as $\sqrt{\omega}$.

In order to be more specific, in the following figures we consider a selected case which may appear in geotechnics and show the normalized velocities of both Rayleigh and Stoneley waves for a permeability coefficient $\pi = 10^7 \frac{\mathrm{kg}}{\mathrm{m^3 s}}$. This corresponds, as shown above, to sandstone saturated with water.

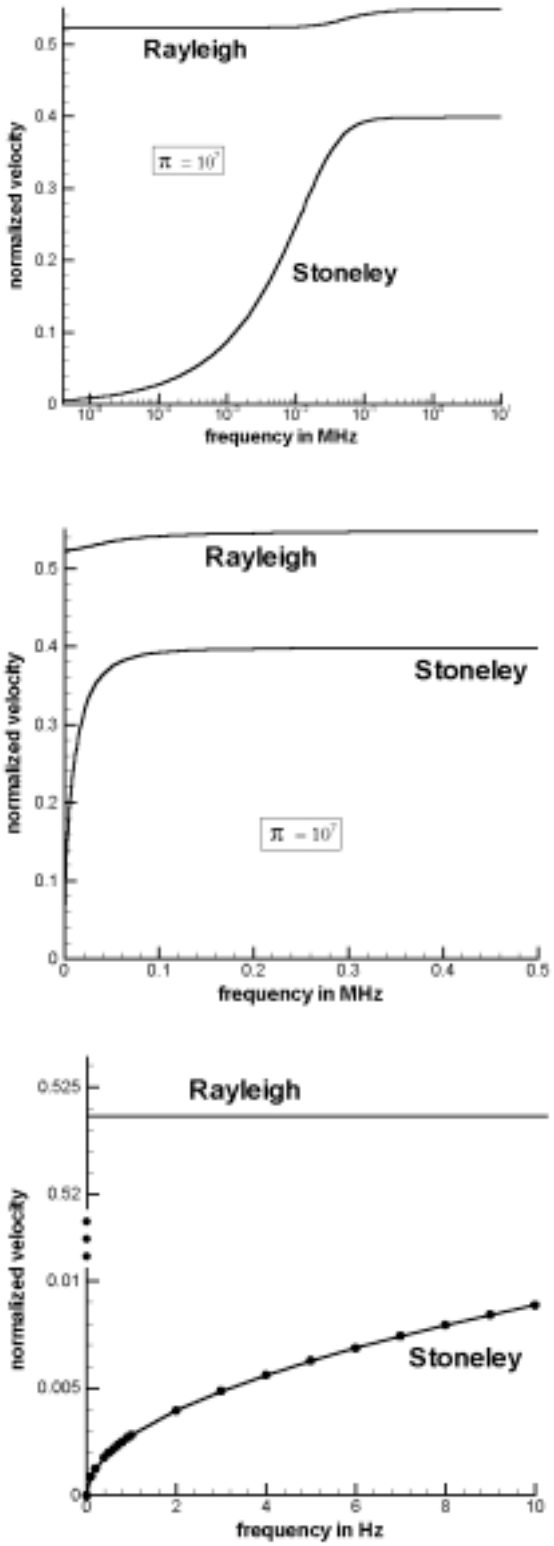


**Fig. 4:** Comparison of the behaviour of Rayleigh and Stoneley wave velocities in different frequency ranges) for a permeability coefficient $\pi = 10^7 \frac{\mathrm{kg}}{\mathrm{m^3 s}}$.

In Fig. 4 we see the velocities of both surface modes in different ranges of frequencies. The first graph shows properties in a large range to 10 MHz in a logarithmic scale while the second one – up to 0.5 MHz, and the third one – up to 10 Hz, both in the normal scale. Each wave attends a finite asymptotic value as $\omega \to \infty$. This value is bigger for the Rayleigh wave than for the Stoneley wave. While the Stoneley wave velocity starts from zero for $\omega = 0$ the Rayleigh wave yields a low frequency limit unequal to zero. With growing frequency the Rayleigh wave remains at first nearly constant and then increases little until it reaches the high frequency limit. On the other hand the growth of the Stoneley wave velocity is much steeper.

In order to demonstrate the existence of the Stoneley wave in the range of very small frequencies, we present in Fig. 4 (the last graph) velocities of this wave for very small values of the frequency (in this figure the frequency is given in Hz while in all other figures the unit of measurement is MHz). It has been earlier solely indicated that the limit of this velocity is zero for $\omega = 0$ [17]. We show some calculated points which make obvious that there do not appear any numerical problems to calculate the Stoneley velocity in the limit $\omega \to 0$. In the same range of frequencies, usual in geophysics, the Rayleigh velocity remains nearly constant. Notice that the velocity axis is broken in order to show the behaviour of both velocities in the same units. For somewhat bigger values of the frequency (the middle graph) one can observe already that both curves tend to their asymptotic values.

## 5.2 Attenuation of Rayleigh and Stoneley waves

This section is devoted to the behaviour of the attenuation of the Rayleigh and Stoneley waves. Imaginary parts of the wave number $k$ determine the damping of waves. It is normalized by the product with the $P1$-velocity and the relaxation time (see: (9)). This means for our parameters that the values presented in the figures are 400 times smaller than in real physical units.

Let us first turn our attention to the Rayleigh wave. Fig. 5 shows the normalized attenuation of this wave. It is obvious that this wave is strongly attenuated. Due to the logarithmic scale it does not emerge from the figures that the attenuation linearly increases to infinity as $\omega \to \infty$ (see Fig. 8, right hand side). Similar to the attenuation of $P1$-waves these curves intersect for different values of $\pi$. The impression one has from the left hand side of Fig. 5, namely that the attenuation would not start from zero with zero frequency stems from the double logarithmic plot of the curves. In the right figure we see (at least at the frequency-axis) the right physical behaviour, namely that the attenuation for all values of $\pi$ starts from zero. The left figure clarifies that the attenuation is in the same manner selfsimilar as the velocity.

In order to expose a practically important region of very small frequencies, we present in Fig. 6 the attenuation of both surface waves and two bulk waves: $P1$ and $P2$ in the range of frequencies up to 1000 Hz. Clearly, in this range, the Rayleigh wave is

attenuated stronger than the $P1$ wave but still weaker than $P2$.

The above analysis reveals a singular behaviour of the Rayleigh wave in relation to the attenuation. Namely, in contrast to all other waves whose attenuation goes to a finite limit as $\omega \to \infty$ – a property which, incidentally, was not clearly stated in earlier works – the attenuation of the Rayleigh wave grows unbounded. This is the feature of a *leaky wave*.

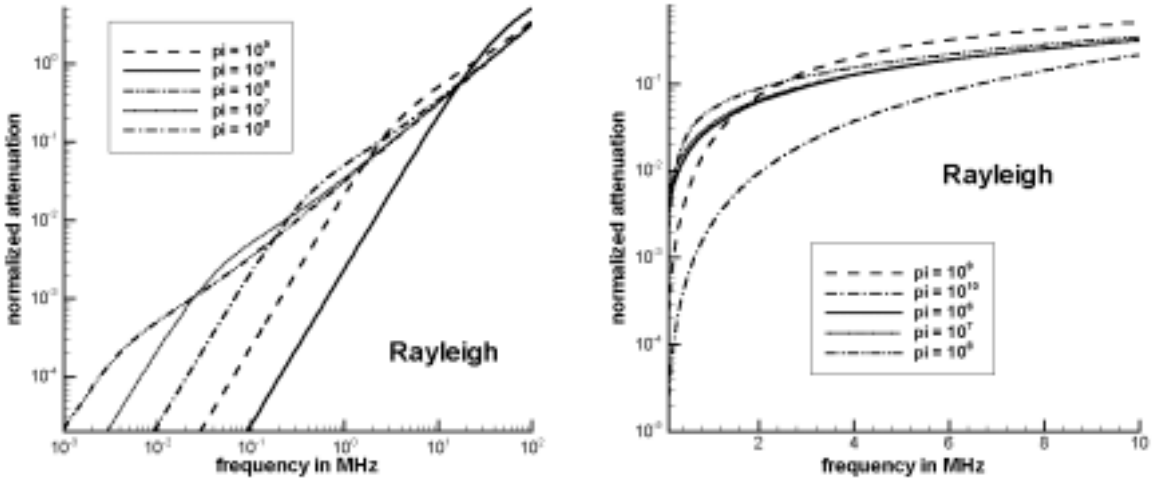


**Fig. 5:** Normalized attenuation of the Rayleigh wave for different values of the permeability coefficient $\pi$ in units $\left[\frac{\mathrm{kg}}{\mathrm{m^3 s}}\right]$ in different ranges of frequencies.

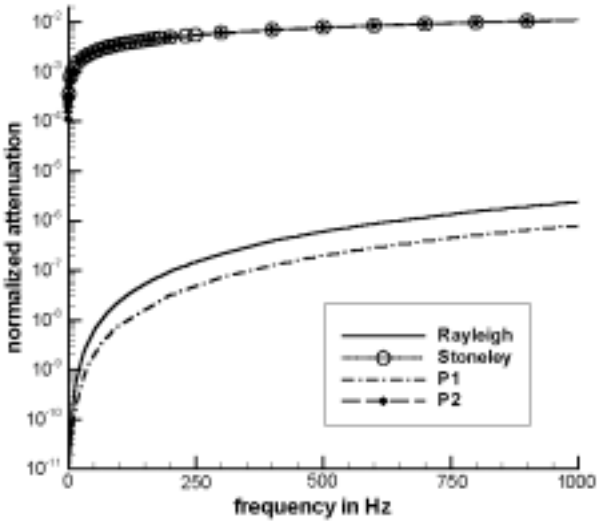


**Fig. 6:** Normalized attenuation of Rayleigh, Stoneley, $P1$ and $P2$-wave, for $\pi = 10^7$ $\frac{\mathrm{kg}}{\mathrm{m^3 s}}$ in a small range of frequencies.

Inspection of Fig. 7 shows that also the normalized attenuation of the Stoneley wave starts from the zero value for $\omega = 0$. But in contrast to the Rayleigh wave attenuation for small frequencies it increases much faster and then approaches a horizontal asymptotic value for larger values of the frequency. This means the limit $\omega \to \infty$ is finite and dependent on the permeability coefficient $\pi$. This property does not coincide with the statement in [7] in which it is claimed that the Stoneley wave propagates "almost without attenuation" (p. 38). This feature concerns the quantity $\operatorname{Im}\tilde{\omega} \equiv \frac{\operatorname{Im}\omega}{k}$ in terms of the quoted paper, and means solely that $\lim\limits_{k\to\infty} \operatorname{Im}\omega < \infty$. In the frequency space considered in the present work we have similarly $\lim\limits_{\omega\to\infty} \operatorname{Im} k < \infty$.

However, we can reinterprete the results in terms of the quality factor used frequently in works on acoustics. As indicated in [1], [4], for instance, it may be defined as

$$Q(\omega) = \left|\frac{\operatorname{Re} k(\omega)}{\operatorname{Im} k(\omega)}\right| \equiv \left|\frac{\operatorname{Re} k(\omega)}{\omega}\frac{\omega}{\operatorname{Im} k(\omega)}\right| = \frac{1}{c_{ph}}\left|\frac{\omega}{\operatorname{Im} k(\omega)}\right|, \quad c_{ph} := \frac{\omega}{\operatorname{Re} k(\omega)}. \quad (32)$$

Clearly, for $|\operatorname{Im} k(\omega)| < \infty$, we have the limit $\lim\limits_{\omega\to\infty} Q(\omega) = \infty$, which is qualified in these works as a lack of dissipation. The other limit $Q = 0$ would mean an infinitely attenuating medium.

We do not use the notion of the quality factor in this work because neither its definition (32) is universally accepted, particularly for the limit $\omega \to 0$, nor it possesses such a clear physical interpretation as $\operatorname{Im} k$.

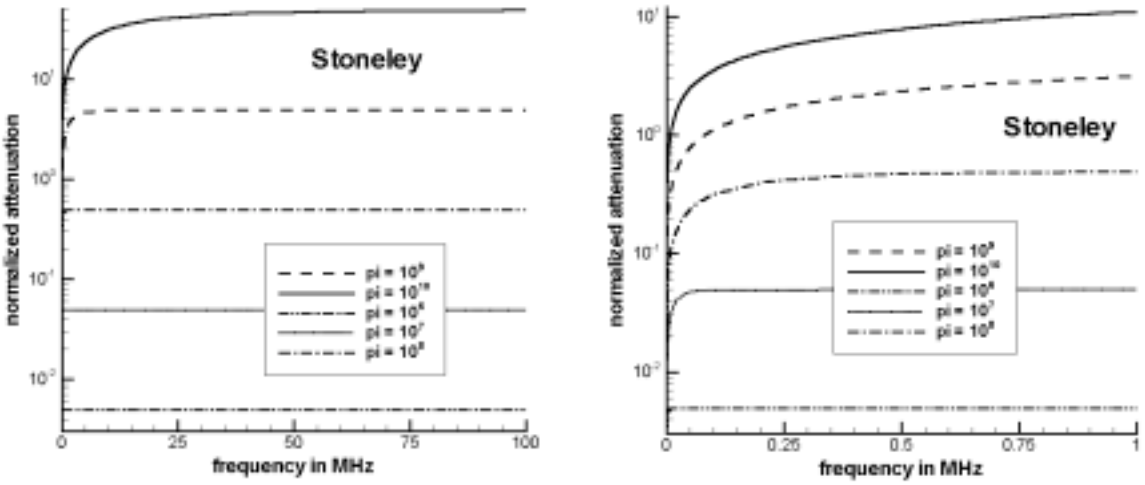


**Fig. 7:** Normalized attenuation of the Stoneley wave for different values of the permeability coefficient $\pi$ in units $\left[\frac{\mathrm{kg}}{\mathrm{m^3 s}}\right]$ in different ranges of frequencies.

In Fig. 8 we show the normalized attenuation of the surface and bulk waves. For low frequencies the attenuation of the Stoneley wave is much higher than this of

the Rayleigh wave. Both attenuations are starting from zero for $\omega = 0$. The Stoneley wave attenuation increases rapidly until it reaches a certain value which depends on the permeability coefficient $\pi$, in the case under consideration – app. $0.0496 \times (c_{P1}\tau)^{-1} \simeq 19.84 \frac{1}{\mathrm{m}}$. After reaching this value – which happens in the low frequency range – it remains constant. The Rayleigh wave attenuation, however, does not have a finite value for $\omega \to \infty$. As we have already mentioned, the Rayleigh wave is for this reason a leaky wave. Generally, the Rayleigh attenuation increases linearly with growing $\omega$ (i.e. the corresponding quality factor $\lim\limits_{\omega \to \infty} Q(\omega) < \infty$), only for very low frequencies the growth is a little bit faster. Consequently, there appears an intersection of the attenuation curves of both waves. This point lies in the range of high frequencies.

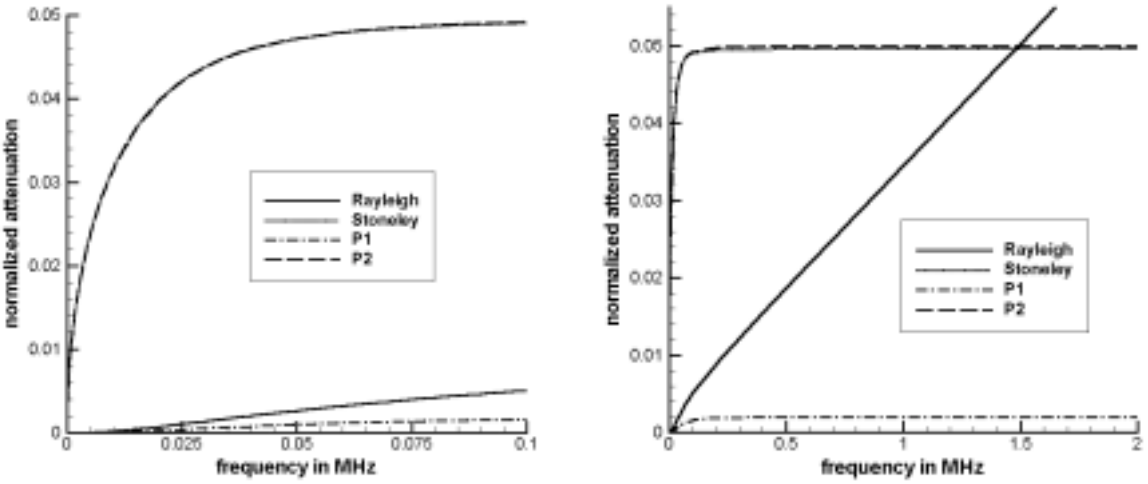


**Fig. 8:** Normalized attenuation of Rayleigh, Stoneley, $P1$ and $P2$-wave, for $\pi = 10^7$ $\frac{\mathrm{kg}}{\mathrm{m^3 s}}$ in different ranges of frequencies.

# 6 Concluding remarks

This work is devoted to the numerical investigation of the dispersion relation for surface waves on an impermeable boundary of a fully saturated poroelastic medium in the *whole range of frequencies*. In the whole range there exist two modes of surface waves corresponding to the classical Rayleigh and Stoneley waves. We have shown numerical results for the normalized velocities $\left(\frac{1}{c_{P1}} \frac{\omega}{\mathrm{Re}\, k(\omega)}\right)$ and attenuations $(\mathrm{Im}\, k(\omega)\, c_{P1}\tau)$ of these waves for different values of the bulk permeability coefficient, $\pi$, in different ranges of frequencies, $\omega$.

**Rayleigh**

- the velocity of propagation of this wave lies in the interval determined by the limits $\omega \to 0$ (following from (31)) and $\omega \to \infty$ (following from (27)). The

high frequency limit is app. 4.7% higher than the low frequency limit. The velocity is always smaller than $c_S$, i.e. slower than the $S$-wave. As a function of $\omega$ it possesses an inflection point and it is slightly nonmonotonous,

- this nonmonotonicity appears in the range of small frequencies. The velocity possesses in this range a minimum whose size is very small (app. 0.025% of the difference of limit values for $\omega = 0$ and $\omega \to \infty$). Interestingly, the minimum value remains constant for the different values of $\pi$. This means that the decay is not driven by the diffusion. Such a behaviour is also observed within Biot's model;
- the attenuation of this wave grows from zero for $\omega = 0$ to infinity as $\omega \to \infty$. In the range of large frequencies it is linear (i.e. the quality factor is a constant different from zero). This means that it is a leaky wave.

**Stoneley**

- the velocity of this wave grows monotonically from the zero value for $\omega = 0$ to a finite limit which is slightly smaller (app. 0.15%) than the velocity $c_{P2}$ of the $P2$-wave. The growth of the velocity of this wave in the range of low frequencies is much steeper than this of Rayleigh waves similarly to the growth of the $P2$-velocity. According to arguments of Bourbié, Coussy, Zinszner [4] this explains the nonmonotonicity of the Rayleigh velocity;
- both the velocity and attenuation of the Stoneley wave approach zero as $\sqrt{\omega}$,
- the attenuation of the Stoneley wave grows monotonically to a finite limit for $\omega \to \infty$. It is slightly smaller than the attenuation of $P2$-waves. Consequently, in contrast to the claims in the literature, the Stoneley wave is attenuated. Solely its quality factor goes to zero as $\omega \to \infty$.

Results for different values of the permeability coefficient $\pi$ are selfsimilar, i.e. a change of $\pi$ yields a corresponding change in the scale of the frequency axis for velocities, and of both axes for attenuations. Otherwise the qualitative behaviour remains unchanged.

The above presented results distort the qualitative behaviour of surface waves because the analysis is two-dimensional. This means that the attenuation has solely a dissipative but not dispersive character. This suppresses the main advantage of surface waves in comparison to bulk waves.

**Acknowledgement:** I appreciate very much numerous valuable discussions with Prof. Dr. K. Wilmański and his help during this work.

# References


[1] K. Aki, P. Richards; *Quantitative seismology, theory and methods*, W. H. Freeman and Co.(1980).

[2] J. Bear; *Dynamics of Fluids in Porous Media*, Dover Publications, New York (1988).

[3] M. A. Biot; *Acoustics, elasticity and thermodynamics of porous media: Twenty-one papers by M. A. Biot*, I. Tolstoy (ed.), American Institute of Physics (1992).

[4] T. Bourbie, O. Coussy, B. Zinszner; *Acoustics of porous media*, Editions Technip, Paris (1987).

[5] H. Deresiewicz; The effect of boundaries on wave propagation in a liquid filled porous solid. IV. Surface waves in a half space, *Bull. Seismol. Soc. Am.*, **52**, 627-638 (1962).

[6] H. Deresiewicz, R. Skalak; On uniqueness in dynamic poroelasticity, *Bull. Seismol. Soc. Am.*, **53**, 783-788 (1963).

[7] I. Edelman, K. Wilmanski; Asymptotic analysis of surface waves at vacuum/porous medium and liquid/porous medium interfaces, *Cont. Mech. Thermodyn.*, 25-44, **14**, 1 (2002).

[8] S. Feng, D.L. Johnson; High-frequency acoustic properties of a fluid/porous solid interface. I. New surface mode, *J. Acoust. Soc. Am.*, **74**(3), 906-914 (1983).

[9] C. Lai; *Simultaneous inversion of Rayleigh phase velocity and attenuation for near-surface site characterization*, PhD-Thesis, Georgia Institute of Technology (1998).

[10] G. J. Rix, C. G. Lai, S. Foti; Simultaneous measurement of surface wave dispersion and attenuation curves, *Geotechnical Testing Journal*, 24(4), 350-358 (2001).

[11] I. A. Viktorov; *Rayleigh and Lamb waves. Physical theory and applications*, Plenum Press, New York (1967).

[12] K. Wilmanski; Waves in porous and granular materials, in: *Kinetic and Continuum Theories of Granular and Porous Media*, K. Hutter, K. Wilmanski (eds.), 131-186, CISM Courses and Lectures No. 400, Springer Wien New York (1999).

[13] K. Wilmanski; Some questions on material objectivity arising in models of porous materials, in: *Rational Continua, classical and new*, M. BROCATO (ed.), 149-161, Springer-Verlag, Italia Srl, Milano (2001).

[14] K. Wilmanski; Note on weak discontinuity waves in linear poroelastic materials. Part I. Acoustic waves in saturated porous media, WIAS-Preprint No. 730 (2002).

[15] K. Wilmanski; Propagation of sound and surface waves in porous materials, in: B. Maruszewski (ed.), *Structured Media*, Poznan University of Technology, Poznan, 312-326 (2002).

[16] K. Wilmanski; Macroscopic modeling of porous and granular materials - microstructure, thermodynamics and some boundary-initial value problems, Keynote Lecture at CANCAM 2003, WIAS-Preprint No. 858 (2003).

[17] K. Wilmanski, B. Albers; Acoustic waves in porous solid-fluid mixtures, in: *Dynamic Response of Granular and Porous Materials under Large and Catastrophic Deformations*, K. Hutter, N. Kirchner (eds.), Lecture Notes in Applied and Computational Mechanics, Vol.11, Springer, Berlin, 285-314 (2003).